Channel Estimation for Reconfigurable Intelligent Surface Assisted Wireless Communication Systems in Mobility Scenarios

Zhendong, Mao, Mugen, Peng, Xiqing, Liu*

State Key Laboratory of Networking and Switching Technology, Beijing University of Posts and Telecommunications, Beijing 100876, China

* The corresponding author, email: liuxiqing@bupt.edu.cn

Abstract: Reconfigurable intelligent surface (RIS) can manipulate the wireless propagation environment by smartly adjusting the amplitude/phase in a programmable panel, enjoying the improved performance. The accurate acquisition of the instantaneous channel state information (CSI) in the cascaded RIS chain makes an indispensable contribution to the performance gains. However, it is quite challenging to estimate the CSI in a time-variant scenario due to the limited signal processing capability of the passive elements embedded in a RIS pannel. In this work, a channel estimation scheme for the RIS-assisted wireless communication system is proposed, which is demonstrated to perform well in a time-variant scenario. The cascaded RIS channel is modeled as a state-space model based upon the mobility situations. In addition, to fully exploit the time correlation of channel, Kalman filter is employed by taking the prior information of channels into account. Further, the optimal reflection coefficients are derived according to the minimum mean square error (MMSE) criterion. Numerical results show that the proposed methods exhibit superior performance if compared with a conventional channel estimation scheme.

Keywords: reconfigurable intelligent surface (RIS); channel estimation; time-variant channel; kalman filter

Received: Aug. 14, 2020
Revised: Nov. 24, 2020
Editor: Shi Jin

I. INTRODUCTION

Recently, the reconfigurable intelligent surface (RIS) technique was suggested to be used in wireless communications due to its promising performance in spectrum/energy efficiency [1–5]. Specifically, RIS is an artificial panel of electromagnetic (EM) material filled with a large array of low-cost passive scattering elements, which can manipulate the wireless environment by adjusting the amplitude or phase shift of reflected signal [6]. Different from the traditional amplify-and-forward (AF) relay, those passive elements consume little energy [7]. Due to this reconfigurable character, RIS can be used to improve the propagation environment and enhance channel quality, even for the high mobility channel, such as unmanned aerial vehicle channels [8].

Plenty of works proved the priority of the RIS-assisted communication systems [9–14]. In [9], a detailed performance analysis of the RIS-assisted single-input single-output communication systems was presented. In that work, a closed-form upper bound of the ergodic capacity was derived, and an accurate approximation of the outage probability was obtained. Numerical results showed that the ergodic capacity and outage probability performances were improved significantly with the increase in number of reflecting elements. In [10], a RIS-assisted single-cell wireless system was developed where the total transmit power minimization problem was formulated and then solved by jointly optimizing beamforming

at the AP and reflection coefficients at the RIS under the constraints of signal-to-interference-plus-noise ratio (SINR). Numerical results demonstrated that a RIS-assisted multiple-input multiple-output (MIMO) system simplified active radio-frequency chains significantly with the same rate performance compared with a benchmark massive MIMO system. In [11], the authors investigated a multi-user MISO downlink communication with the aid of RIS. The transmit powers and the reflection coefficients are jointly designed for sum-rate maximization subject to individual QoS guarantees. Numerical results showed that RIS improved system throughput by at least 40 percent. The multi-user MISO downlink communication was discussed in [12], where the energy-efficient designs were studied for both the transmit power allocation and the phase shifts of the surface reflecting elements. Numerical results proved that the proposed RIS-based resource allocation methods obtained 300 percent higher energy efficiency than a regular AF relay based resource allocation. In [13], the fundamental capacity limit of RIS-assisted point-to-point MIMO communication systems was characterized by jointly optimizing the RIS reflection coefficients, and the MIMO transmit covariance matrix. Numerical results demonstrated that the capacity was substantially increased with the assistance of RIS.

However, the works mentioned above mainly focus on the designs and optimizations of the reflection coefficients under the assumption that the channel state informations (CSIs) are perfectly known. In practice, the acquisition of CSI is quite a challenging issue owing to two facts [15]. For one thing, the passive elements in an RIS panel can not perform active signal processing, and hence RIS is unable to send training sequences independently. As a result, the CSIs have to be estimated at the BS/user sides. For another, the massive passive elements in RIS introduce a large number of unknown channel parameters, which requires a high overhead for channel estimation.

Some efforts have made to achieve the accurate CSIs in RIS-assisted systems [15–21]. In [15], an RIS-enhanced orthogonal frequency division multiplexing (OFDM) system was considered, and a transmission protocol was proposed to execute channel estimation and reflection optimization successively. A novel reflection pattern was then designed for channel estimation under the unit-modulus constraint; meanwhile, the reflection coefficients are optimized with the estimated CSI. To reduce the overhead for channel estimation, the authors in [16] proposed a novel element grouping method to exploit the channel spatial correlation in an RIS-assisted OFDM system under frequency-selective channels. A practical transmission protocol with the on/off strategy was then designed. After that, the alternative optimization method was utilized to maximize the achievable rate by jointly optimizing the BS's power allocation and the RIS's passive beamforming iteratively. In [17], a general framework for the estimation of the transmitter-RIS and RIS-receiver cascaded channel was introduced. A two-stage algorithm consisting of a sparse matrix factorization stage and a matrix completion stage was proposed. In [18], the channel estimation for the RIS-assisted multiuser MIMO system was formulated as a matrix-calibration based matrix factorization task. A novel message-passing algorithm was constructed based on the slow-varying channel components and the hidden channel sparsity. By exploring the properties of Katri-Rao, Kronecker products and wireless channels' sparsity, the cascaded channel estimation was formulated in [19] as a sparse signal recovery problem. Different from previous works, the authors in [20] introduced a deep learning framework for channel estimation in RIS-assisted massive MIMO systems. With the trained convolutional neural network architecture, both direct and cascaded channels can be estimated by the received pilot signals.

However, the RIS-assisted wireless system with a time-variant channel is not studied sufficiently in existing researches, and this kind of system particularly needs the help of RIS to improve its channel quality. Motivated by this reason, in this paper, we consider an RIS assisted uplink wireless communication system, where the User-RIS link channel is regarded as a time-variant channel due to the high mobility of users. A feasible transmission protocol is proposed, and the cascaded channel can then be regarded as a state-space model. In order to capture the time-variant characteristic, the Kalman filter is applied to estimate the cascaded channel. The reflection coefficient matrix is then optimized based on the minimum mean square error (MMSE) criterion. The main contributions of this paper are summarized as follows:

- In order to capture the time-variant characteristic, a feasible transmission protocol is proposed

to adapt to the two-scaling channel, and the cascaded channel is modeled as a state-space model.

- The Kalman filter is employed to improve the estimation accuracy by tracking the channel variation over time according to prior knowledge of the temporal correlation coefficient. Meanwhile, the optimal reflection coefficient matrix is derived based on the MMSE criterion.
- Numerical results are carried out to demonstrate the superiority and accuracy of the proposed methods.

The rest of the paper is organized as follows: In Section II, the system model, including the RIS-based channel and signal transmission, is introduced in detail. In Section III, we will first introduce the Kalman filter scheme, which is used to estimate the CSI of the RIS involved wireless channel. Additionally, the optimization algorithm with respect to the reflection coefficient is derived therein. Numerical results are presented in Section IV, followed by the conclusions in Section V.

Notations: Uppercase and lowercase boldface denote matrices and vectors, respectively. The operators $\mathbf{A}^T$, $\mathbf{A}^H$, $\mathbf{A}^{-1}$ refer to the transpose, conjugate transpose, and inverse, respectively. $\mathbf{I}_N$ stands for an $N \times N$ identity matrix. $\mathbb{C}^{M\times N}$ ($\mathbb{R}^{M\times N}$) denotes the $M \times N$ dimensional complex (real) vector space. $\mathcal{CN}(\mathbf{a}, \mathbf{B})$ stands for the circular symmetric complex Gaussian distribution with its mean to be $\mathbf{a}$ and covariance to be $\mathbf{B}$, respectively. The diagonal matrix is denoted by $\mathrm{diag}(\mathbf{x})$ with elements of $\mathbf{x}$ on its diagonal and $\mathrm{tr}(\mathbf{X})$ represents the trace of matrix $\mathbf{X}$. $\|\mathbf{A}\|_F$ denotes the Frobenius norm of $\mathbf{A}$.

II. SYSTEM MODEL

In this work, we focus on the uplink time-variant wireless channels, where the user is connected to the BS with the assistance of a reconfigurable intelligent surface (RIS), as shown in Figure 1. The BS is equipped with M antennas, and the user is equipped with one antenna. The RIS consists of N passive reflecting elements with their amplitude and phase adjustable. The RIS is connected to a smart controller to enable dynamic adjustment of its elements individual reflections. In this paper, only the User-RIS-BS reflecting link is our focus. The channel estimation for the direct link is not our concern since sufficient solutions can be found in the existing works [15].

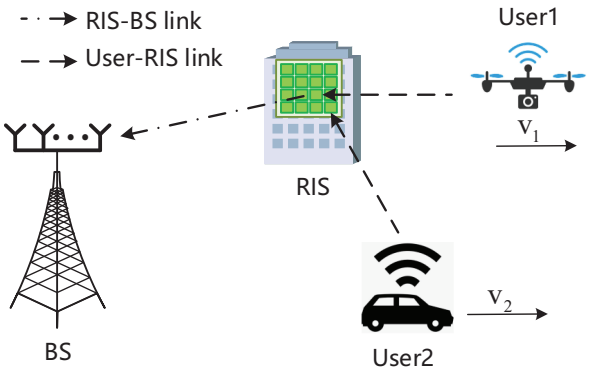

Figure 1. *The RIS-assisted channel model used in this work. In this model, BS and RIS keep static; while the users are in mobility.*

2.1 Channel Model

Define $\mathbf{h} \in \mathbb{C}^{N\times 1}$ as the channel vector between RIS and user, with its coherence time to be T_h; while $\mathbf{G}^H \in \mathbb{C}^{M\times N}$ is the channel matrix between BS and RIS whose coherence time is denoted by T_g. In our model, the BS and RIS keep static and the user is moving fast, and then it can be assumed $T_g > T_h$. Further, we assume $T_g = I \cdot T_h$ and the channels $\mathbf{h}$ and $\mathbf{G}$ remain constant within their coherence time, as shown in Figure 2.

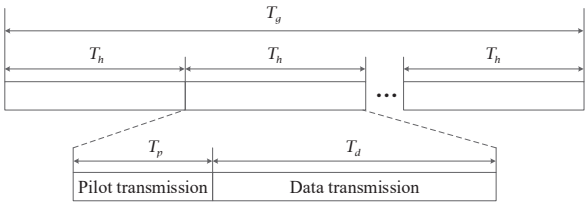

Figure 2. *Illustration of the channel coherence time. Define T_g and T_h as the coherent times for the BS-RIS link and RIS-User link, respectively. Also, a reasonable assumption that T_h is much shorter than T_g is built on the different mobility states. In addition, within T_h, the signaling can be divided into pilot transmission and data transmission, respectively.*

Taking T_h as the reference slot, the channel $\mathbf{G}$ satisfies

$$\mathbf{G}_1 = \mathbf{G}_2 = \cdots = \mathbf{G}_I = \mathbf{G}, \tag{1}$$

where $\mathbf{G}$ is assumed to be Rayleigh channel in this work, whose elements are complex Gaussian variants with zero mean and unit variance, respectively.

The channel $\mathbf{h}$ is modeled as the time-variant channel according to a first-order time varying autoregressive (AR) process [22, 23]

$$\mathbf{h}_i = \mathbf{A}_{i-1}\mathbf{h}_{i-1} + \mathbf{v}_{i-1}, \quad i = 1, 2, ..., I, \tag{2}$$

where $\mathbf{A}_{i-1} = \text{diag}(\alpha_{i-1,1}, \alpha_{i-1,2}, ..., \alpha_{i-1,N})$ is the frequency response state transition matrix in the $(i-1)$th slot and $\mathbf{v}_{i-1} \in \mathbb{C}^{N\times 1}$ stands for the model error, whose elements are additive Gaussian noise with means to be zero and variances to be σ_v^2, respectively.

The element in $\mathbf{A}_{i-1}$, i.e. $\alpha_{i,n}$ is the time-correlation coefficient, which can be written into

$$\alpha_{i,n} = \alpha = J_0(2\pi f_d T_h), \tag{3}$$

where J_0 denotes the zero-order Bessel function of the first kind. Also, f_d is the maximum Doppler frequency shift, and the variance $\sigma_v^2 = 1 - a^2$ ensures that the channel $\mathbf{h}_i$ maintains the same power level.

The reason for (3) is that as the time-correlation characteristics of different elements in the same RIS are similar, we define $\alpha_{i,n} = \alpha_i$ for compact expression. Also, the time-correlation coefficient between the ith slot and the i'th slot, denoted by $\alpha = J_0(2\pi f_d|i-i'|T_h)$, is mainly decided by $|i-i'|T_h$. In our work, only the adjacent two slots, i.e. the $(i-1)$th slot and the ith slot are considered for the current ith slot. Therefore, we can have $\alpha_i = \alpha = J_0(2\pi f_d T_h)$, which is independent of i.

Then, Eq. (2) can be rewritten as

$$\mathbf{h}_i = \alpha\mathbf{h}_{i-1} + \mathbf{v}_{i-1}, \quad i = 1, 2, \cdots, I. \tag{4}$$

2.2 Signal Model

In order to improve the estimation accuracy, a transmission protocol is designed in this work, as shown in Figure 3. A reference slot T_h is divided into two parts, where the head T_p symbols are dedicated for pilot training and the subsequent $T_d = T_h - T_p$ symbols are utilized for data transmission.

In the head T_p symbols, the RIS adjusts the reflection vector $\boldsymbol{\phi}^{(j)}$ in the jth symbol in order to assist the channel estimation. With the estimated CSI, the RIS can obtain the optimized reflection vector $\boldsymbol{\psi}_i$ for data transmission. Therefore, the reflection coefficient $\boldsymbol{\psi}_i$ keeps constant during data transmission.

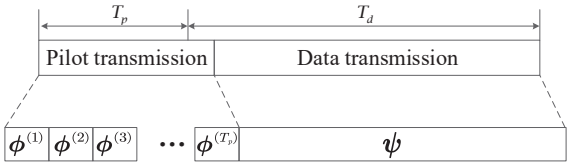

Figure 3. *Illustration of the transmission protocol, with the head T_p symbols for pilot training and the subsequent $T_d = T_h - T_p$ symbols for data transmission.*

The received signal vector $\mathbf{y}_i^{(j)} \in \mathbb{C}^{M\times 1}$ at the jth symbol in the ith slot can be expressed as

$$\begin{aligned}\mathbf{y}_i^{(j)} &= \sqrt{P_t}\mathbf{G}^H \text{diag}(\boldsymbol{\phi}_i^{(j)})\mathbf{h}_i s_i + \mathbf{w}_i^{(j)} \\ &\overset{(a)}{=} \sqrt{P_t}\mathbf{G}^H \text{diag}(\mathbf{h}_i)\boldsymbol{\phi}_i^{(j)} s_i + \mathbf{w}_i^{(j)},\end{aligned} \tag{5}$$

where P_t is the transmit power, and $s_i \in \mathbb{C}$ represents the training signal. Besides, $\mathbf{w}_i^{(j)} \in \mathbb{C}^{M\times 1}$ stands for the complex Gaussian noise with zero mean and unit variance. In addition, $\boldsymbol{\phi}_i^{(j)} = \frac{1}{\sqrt{N}}[\phi_{i,1}^{(j)}, \phi_{i,2}^{(j)}, \cdots, \phi_{i,N}^{(j)}]^H$ represents the reflection vector of the RIS at the jth symbol in the ith slot, whose element $|\phi_{i,n}^{(j)}| \leq 1$ is the reconfigurable reflection coefficient on the nth reflective element. The equation sign of (a) holds due to the fact that $\forall \mathbf{a}, \mathbf{b} \in \mathbb{C}^{N\times 1}$, $\text{diag}(\mathbf{a})\mathbf{b} = \text{diag}(\mathbf{b})\mathbf{a}$.

Define

$$\begin{aligned}\mathbf{Y}_i &\triangleq [\mathbf{y}_i^{(1)}, \mathbf{y}_i^{(2)}, \cdots, \mathbf{y}_i^{(T_p)}], \\ \boldsymbol{\Phi}_i &\triangleq \sqrt{P_t}[\boldsymbol{\phi}_i^{(1)}, \boldsymbol{\phi}_i^{(2)}, \cdots, \boldsymbol{\phi}_i^{(T_p)}], \\ \mathbf{W}_i &\triangleq [\mathbf{w}_i^{(1)}, \mathbf{w}_i^{(2)}, \cdots, \mathbf{w}_i^{(T_p)}]\end{aligned}$$

and omit s_i for the sake of simplicity. Then, Eq. (5) can be rewritten as

$$\mathbf{Y}_i = \mathbf{G}^H \text{diag}\left(\mathbf{h}_i\right) \boldsymbol{\Phi}_i + \mathbf{W}_i. \tag{6}$$

Taking the transpose operation on both sides of (6), we can obtain that

$$\begin{aligned}\mathbf{Y}_i^T &= \boldsymbol{\Phi}_i^T \text{diag}\left(\mathbf{h}_i\right) \mathbf{G}^* + \mathbf{W}_i^T \\ &= \boldsymbol{\Phi}_i^T \mathbf{D}_i + \mathbf{W}_i^T,\end{aligned} \tag{7}$$

where $\mathbf{D}_i = \text{diag}(\mathbf{h}_i)\mathbf{G}^* \in \mathbb{C}^{N\times M}$ is the cascaded channel to be estimated. Further, transforming the vector into diagonal matrix on both sides of (4), we

can rewritten (4) as

$$\mathrm{diag}\left(\mathbf{h}_i\right) = \alpha \mathrm{diag}\left(\mathbf{h}_{i-1}\right) + \mathrm{diag}\left(\mathbf{v}_{i-1}\right). \quad (8)$$

After a few simple derivations, we can finally get the state-space model, which is mathematically described as

$$\begin{cases} \mathbf{Y}_i^T = \mathbf{\Phi}_i^T \mathbf{D}_i + \mathbf{W}_i^T, \\ \mathbf{D}_i = \alpha \mathbf{D}_{i-1} + \mathrm{diag}\left(\mathbf{v}_{i-1}\right) \mathbf{G}^*. \end{cases} \quad (9)$$

In the data transmission stage, the received data signal $\mathbf{\Upsilon}_i$ at the ith slot can be expressed by

$$\begin{aligned} \mathbf{\Upsilon}_i &= \sqrt{P_d}\mathbf{G}^H \mathrm{diag}(\boldsymbol{\psi}_i)\mathbf{h}_i\mathbf{x}_i + \mathbf{\Omega}_i \\ &= \sqrt{P_d}\mathbf{G}^H \mathrm{diag}(\mathbf{h}_i)\boldsymbol{\psi}_i\mathbf{x}_i + \mathbf{\Omega}_i \\ &= \sqrt{P_d}\mathbf{D}_i^T \boldsymbol{\psi}_i\mathbf{x}_i + \mathbf{\Omega}_i, \end{aligned} \quad (10)$$

where $\mathbf{x}_i \in \mathbb{C}^{1\times T_d}$ is the signal vector with the power constraint of $\mathrm{tr}(\mathbf{x}_i^H\mathbf{x}_i) = T_d$. Additionally, P_d is the data transmit power, and $\boldsymbol{\psi}_i$ is the reflection coefficient vector for data transmission. $\mathbf{\Omega}_i$ is the complex Gaussian noise matrix whose element has zero mean and unit variance.

Based on the estimated CSI $\hat{\mathbf{D}}_i$, the RIS reflection coefficients can be optimized at the BS to maximize the achievable rate, which is given by

$$\boldsymbol{\psi}_i^{\mathrm{opt}} = \arg\max_{\boldsymbol{\psi}_i} \frac{T_d}{T_p+T_d}\log\left[1+\frac{P_d\mathbb{E}\mathrm{tr}\left(\hat{\mathbf{D}}_i^*\hat{\mathbf{D}}_i^T\boldsymbol{\psi}_i\boldsymbol{\psi}_i^H\right)}{P_d\mathbb{E}\mathrm{tr}\left(\tilde{\mathbf{D}}_i^*\tilde{\mathbf{D}}_i^T\boldsymbol{\psi}_i\boldsymbol{\psi}_i^H\right)+M}\right], \quad (11)$$

where $\tilde{\mathbf{D}}_i \triangleq \mathbf{D}_i - \hat{\mathbf{D}}_i$ is the estimation error.

According to (11), it is straightforward to see that the estimated cascaded channel $\hat{\mathbf{D}}_i$ is necessary for the design of reflection coefficient vector and the data detection; while the individual CSIs of User-RIS and RIS-BS links are not a must for the channel estimation. Our focus in this work is the channel estimation design, and the optimization algorithm of the RIS reflection coefficients for data transmission remains to be solved in future work.

III. CHANNEL ESTIMATION

In this section, the Kalman filter is utilized to estimate the cascaded CSI by exploiting the channel correlation characteristic. According to the minimum mean square error (MMSE) criterion, the optimization of the reflection coefficient is derived to improve the estimation accuracy.

For the linear channel estimation methods, such as least square (LS) and MMSE, only the CSI with the current received training signal is exploited while ignoring the prior information. Although a good estimation accuracy can be achieved with the linear channel estimation in a time-invariant scenario, the outdated CSI is always generated due to the mobility. In this paper, to fully exploit the correlation, the Kalman filter is adopted to estimate the CSI with the current received signal plus the previous signals. The main steps for the Kalman filter based on (9) are summarized in Algorithm 1, where the prior covariance is defined as $\widetilde{\mathbf{P}}_i \triangleq \mathbb{E}\{\|\widetilde{\mathbf{D}}_i - \mathbf{D}_i\|_F^2\}$ and the posterior covariance is defined as $\hat{\mathbf{P}}_i \triangleq \mathbb{E}\{\|\hat{\mathbf{D}}_i - \mathbf{D}_i\|_F^2\}$.

Algorithm 1. *Kalman filter.*

1: **Initialization:**
Initialize $\hat{\mathbf{D}}_0 = \mathbf{0}$, and $\hat{\mathbf{P}}_0 = M\mathbf{I}_N$
2: **Prediction:**
Use $\hat{\mathbf{D}}_{i-1}$ to predict the cascaded CSI in the ith slot, i.e. $\widetilde{\mathbf{D}}_i = \alpha\hat{\mathbf{D}}_{i-1}$;
Calculate the prior covariance, that is,
$\widetilde{\mathbf{P}}_i = \alpha^2\hat{\mathbf{P}}_{i-1} + M(1-\alpha^2)\mathbf{I}_N$;
3: **Optimization:**
Calculate the Kalman gain matrix:
$\mathbf{K}_i = \widetilde{\mathbf{P}}_i\mathbf{\Phi}_i^*(\mathbf{\Phi}_i^T\widetilde{\mathbf{P}}_i\mathbf{\Phi}_i^* + M\mathbf{I}_{T_p})^{-1}$;
Calculate the posterior estimate:
$\hat{\mathbf{D}}_i = \widetilde{\mathbf{D}}_i + \mathbf{K}_i(\mathbf{Y}_i^T - \mathbf{\Phi}_i^T\widetilde{\mathbf{D}}_i)$;
Calculate the posterior covariance:
$\hat{\mathbf{P}}_i = (\mathbf{I} - \mathbf{K}_i\mathbf{\Phi}_i^*)\widetilde{\mathbf{P}}_i$

The MSE of the ith slot is defined as $\mathrm{MSE}_i \triangleq \mathrm{tr}(\hat{\mathbf{P}}_i)$, which is function of reflection matrix $\mathbf{\Phi}_i$.

In order to obtain the optimal reflection matrix $\mathbf{\Phi}_i$ to minimize the MSE, the optimization problem based on $\mathbf{\Phi}_i$ can be written as

$$\begin{aligned} &\min_{\mathbf{\Phi}_i} \mathrm{MSE}_i = \mathrm{tr}\left(\hat{\mathbf{P}}_i\right), \\ &s.t.\ \mathrm{tr}\left(\mathbf{\Phi}_i\mathbf{\Phi}_i^H\right) \le T_pP_t. \end{aligned} \quad (12)$$

Lemma 1. *The optimal reflection coefficient matrix, defined as $\mathbf{\Phi}_i$, satisfies $\mathbf{\Phi}_i^H\mathbf{\Phi}_i = P_t\boldsymbol{I}_{T_p}$.*

Proof. We first consider the MSE in the first slot, i.e.

MSE_1, which can be written as

$$\mathrm{MSE}_1 = MN - M \cdot \mathrm{tr}\left(\mathbf{\Phi}_1^T \mathbf{\Phi}_1^* \left(\mathbf{\Phi}_1^T \mathbf{\Phi}_1^* + \mathbf{I}_{T_p}\right)^{-1}\right). \tag{13}$$

Define $\mathbf{X}_i$ as $\mathbf{X}_i \triangleq \mathbf{\Phi}_i^T \mathbf{\Phi}_i^*$, and we can conclude $\mathbf{X}_i$ is a positive semi-definite Hermitian matrix. Then, Eq. (13) can be further expressed by

$$\mathrm{MSE}_1 = MN - M \cdot \mathrm{tr}\left(\mathbf{X}_1 (\mathbf{X}_1 + \mathbf{I}_{T_p})^{-1}\right). \tag{14}$$

It is known that for a Hermitian matrix $\mathbf{A}$ together with its eigenvector $\mathbf{b}$, there exists a unitary matrix $\mathbf{U}$, yielding $\mathbf{A} = \mathbf{U}\mathrm{diag}(\mathbf{b})\mathbf{U}^H$. According to this property, we can have $\mathbf{X}_i = \mathbf{U}_i \mathrm{diag}(\mathbf{b}_i)\mathbf{U}_i^H$, where $\mathbf{b}_i$ is eigenvector of $\mathbf{X}_i$. Then, Eq. (14) can be simplified into

$$\begin{aligned}\mathrm{MSE}_1 &= MN - M \cdot \mathrm{tr}\left[\mathrm{diag}\left(\mathbf{b}_1\right)\left(\mathrm{diag}\left(\mathbf{b}_1\right) + \mathbf{I}_{T_p}\right)^{-1}\right] \\ &= MN - M \sum_{t=1}^{T_p} \frac{b_{1,t}}{b_{1,t}+1}.\end{aligned} \tag{15}$$

The optimization problem of (12) can be finally rewritten into

$$\begin{aligned} &\min_{\mathbf{b}_1} \ \mathrm{MSE}_i = MN - M \sum_{t=1}^{T_p} \frac{b_{1,t}}{b_{1,t}+1}, \\ &s.t. \ \sum_{t=1}^{T_p} b_{1,t} \le T_p P_t, \\ &\quad b_{1,t} \ge 0, t = 1, 2, \cdots, T_p. \end{aligned} \tag{16}$$

It is easily to know that (16) is a convex optimization problem, and the corresponding Lagrangian function is

$$\begin{aligned}\mathcal{L}\left(\mathbf{b}_1, \lambda_1\right) =& MN - M \sum_{t=1}^{T_p} \frac{b_{1,t}}{b_{1,t}+1} \\ &- \lambda_1 \left(\sum_{t=1}^{T_p} b_{1,t} - T_p P_t\right),\end{aligned} \tag{17}$$

where λ_1 is the Lagrangian multiplier.

Next the Karush-Kuhn-Tucker (KKT) condition is used here, which is summarized as

$$\frac{\partial \mathcal{L}}{\partial b_{1,t}} = -M \frac{1}{(b_{1,t}+1)^2} + \lambda_1, \ t = 1, 2, ..., T_p, \tag{18a}$$

$$\lambda_1 \left(\sum_{t=1}^{T_p} b_{1,t} - T_p P_t\right) = 0, \tag{18b}$$

$$\sum_{t=1}^{T_p} b_{1,t} - T_p P_t \le 0. \tag{18c}$$

For (18a), we can obtain that the optimal $\mathbf{b}_1$, denoted by $\mathbf{b}_{1,\mathrm{opt}}$, should satisfy

$$\lambda_1 (b_{1,t,\mathrm{opt}} + 1)^2 = M, \ t = 1, 2, ..., T_p, \tag{19}$$

in which $\mathbf{b}_{1,\mathrm{opt}}$ can be further written into

$$b_{1,t,\mathrm{opt}} = \sqrt{\frac{M}{\lambda_1}} - 1, \ t = 1, 2, ..., T_p. \tag{20}$$

Then, two situations are investigated depending on whether λ_1 equals to zero or not. For $\lambda_1 = 0$, we can have $\lambda_1 (b_{1,t,\mathrm{opt}} + 1)^2 = 0$, which is violated with (19). For $\lambda_1 \neq 0$, we can get $\sum_{t=1}^{T_p} b_{1,t} = T_p P_t$. According to (20), $\mathbf{b}_{1,\mathrm{opt}}$ is finally expressed by

$$\mathrm{diag}\left(\mathbf{b}_{1,\mathrm{opt}}\right) = P_t \mathbf{I}_{T_p}, \tag{21}$$

Therefore, the optimal $\mathbf{X}_1$, defined as $\mathbf{X}_{1,\mathrm{opt}}$, is given by

$$\mathbf{X}_{1,\mathrm{opt}} = \mathbf{U}_1 \mathrm{diag}(\mathbf{b}_{1,\mathrm{opt}}) \mathbf{U}_1^H = P_t \mathbf{I}_{T_p}. \tag{22}$$

For the subsequent time slots, i.e. $i \ge 2$, the posterior covariance $\hat{\mathbf{P}}_i, i \ge 2$ is exactly similar to $\hat{\mathbf{P}}_1$. As a result, we can straightforwardly draw the conclusion that the optimal solution of $\mathbf{\Phi}_i$ should satisfy $\mathbf{\Phi}_i^T \mathbf{\Phi}_i^* = P_t \mathbf{I}_{T_p}$, $i = 2, \cdots, I$. Therefore, any matrix with orthogonal rows of the same norm $\sqrt{P_t}$ can be regarded as the optimal solution of $\mathbf{\Phi}_i$. This conclusion is also applicable for traditional LS and MMSE estimators. The proof has been finished.

With the optimal $\mathbf{\Phi}_i$ and $T_p = N$, the MSE of the

Kalman filter can be expressed by

$$\mathrm{MSE}_i = \mathrm{tr}\left(\mathbf{P}_i\right) = \frac{MN}{P_t + 1/\beta_i}, \tag{23}$$

where β_i and β_1 equal to $\beta_i = \frac{\alpha^2}{P_t+1/\beta_{i-1}} + 1 - \alpha^2, i \geq 2$ and $\beta_1 = 1$, respectively.

IV. NUMERICAL RESULTS AND DISCUSSIONS

In this section, we will present the performance evaluations for our proposed reflection matrix with Kalman filter through the numerical experiments. The results are obtained over 5000 Monte Carlo trials. The transmit SNR is defined as P/σ_n^2, and the number of passive elements in an RIS is $N = 64$. In order to reduce the overhead of channel estimation, the adjacent elements in the RIS are grouped into a sub-surface sharing a common reflection coefficient due to the high spatial correlation [15]. In our numerical experiments, each sub-surface consists of 4 passive elements. It is indicated that only $\overline{N} = 16$ channels need to be estimated. The lengths of the coherence time for $\mathbf{h}$ and $\mathbf{G}$ are assumed to be $T_h = 50$ and $T_g = 500$, respectively. The mobile velocity of the user is assumed to be 300 km/h. The carrier frequency is 2.6 GHz. The optimal reflection coefficient matrix is set to be a normalized submatrix of the discrete Fourier transform (DFT) matrix [24].

Specifically, we define the normalized MSE (NMSE) as the performance metric, which is given by

$$\mathrm{NMSE} = \mathbb{E}\left[\frac{\|\mathbf{D}_i - \hat{\mathbf{D}}_i\|_F^2}{\|\mathbf{D}_i\|_F^2}\right]. \tag{24}$$

In Figure 4, the NMSE versus the time slot index is given, where both the theoretical and numerical results are presented. As shown in Figure 4, the numerical results are observed keeping consistent with the theoretical curves with SNR being 0 and 10 dB. The Kalman filter estimator utilizes the prior information and the time correlation to estimate the CSI, and hence we can find the NMSEs of both the theoretical and numerical values decrease along with the increase of time slot index. Moreover, the impacts of the reflection coefficient matrices on the NMSE are investigated. The optimal reflection coefficient matrix and the random reflection coefficient matrix are derived from Eqs. (22) and (12), respectively. It is seen that the optimal reflection coefficient matrix significantly outperforms the random reflection coefficient matrix, and it can be proved by Lemma 1.

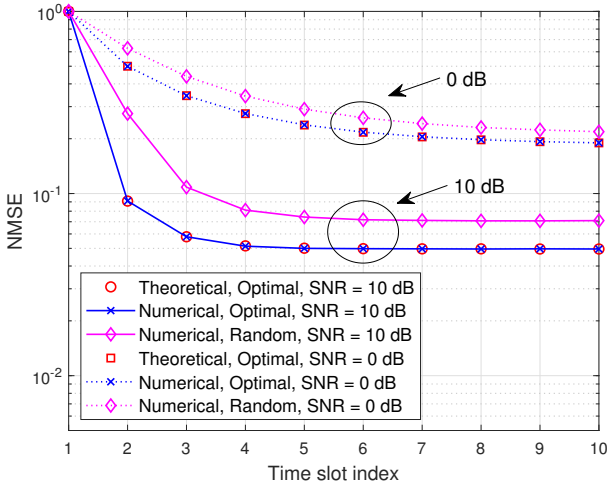

Figure 4. *NMSE versus time slot index for both theoretical and numerical cases. Define M as the number of antennas at BS, which equals to 8.*

In Figure 5, we compare the estimation accuracies among different channel estimators, where the traditional LS, MMSE [25] and the proposed Kalman filter estimators are taken into our numerical experiments. KF-MMSE and KF-LS stand for the Kalman filter's initialization based on MMSE and LS algorithms, respectively. It can be seen from Figure 5 that the NMSEs of KF-MMSE and KF-LS decreases significantly along with the increases of time slot index. Instead, the NMSEs of MMSE and LS receive little impacts of an increase in the time slot index. This is because the Kalman filter utilizes the channel's prior information and channel correlation to improve the estimation accuracy, and the LS and MMSE only exploit the current channel.

Figure 6 shows the NMSE performance of different channel estimators versus SNR. As observed from Figure 6, the Kalman filter estimator owns the best performance, while the LS has low estimation accuracy. Meanwhile, the estimation error for all those estimators reaches unanimity with the increase of SNR. This is because that when SNR is low, the effect of noise gives a dominant influence on estimation performance.

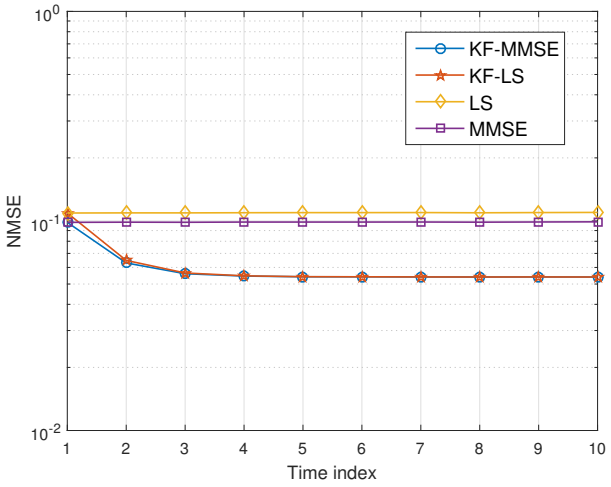

Figure 5. *NMSE versus time index with different channel estimators.*

It is accepted that LS estimator is vulnerable to noise, and thus we can find that it performs poorly in a low SNR zone. MMSE and Kalman filter estimators can suppress noise to a satisfying extent, exhibiting a low NMSE. In the high SNR zone, the effect of noise can be almost ignored, and hence we can observe the three estimators converge the same NMSE.

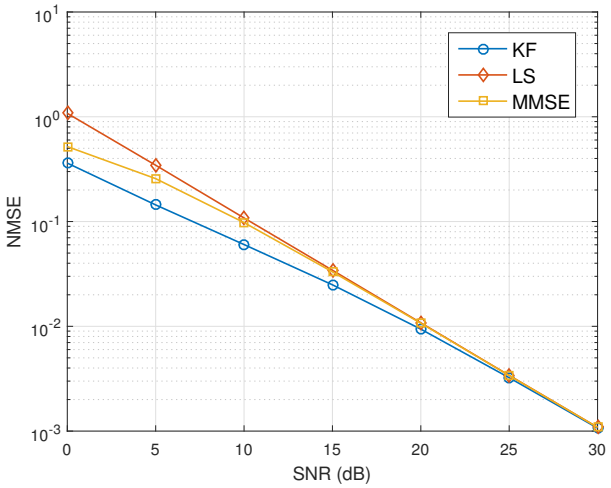

Figure 6. *NMSE versus SNR with different channel estimators.*

In Figure 7, the bit error rate (BER) performance is investigated with different channel estimators, where the quadrature phase shift keying (QPSK) modulation and zero forcing (ZF) equalization are adopted. As shown in Figure 7, we can observe Kalman filter estimator exhibits a better BER performance than the MMSE estimator, as the Kalman filter always owns much attractive estimation accuracy than MMSE in time-variant channels. Also, it is seen the BER with "$M = 128$" is much lower than the BER with "$M = 8$" and the slope of the former is steeper than that of the latter due to the larger diversity gain can be achieved.

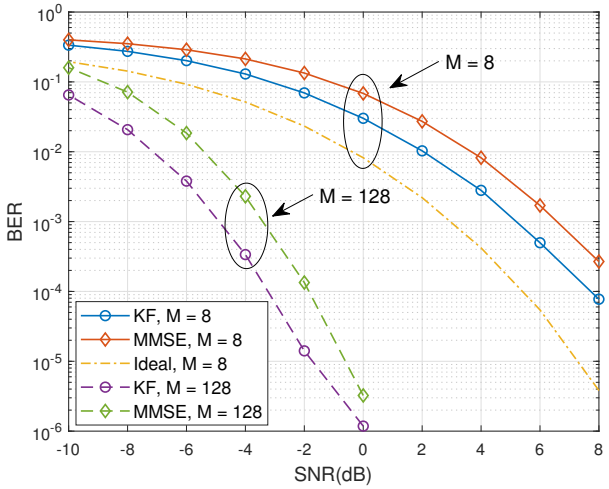

Figure 7. *BER versus SNR with different number of antennas. In this numerical experiment, let the antenna number at BS, defined as M, be 8.*

V. CONCLUSION

In this work, we investigate the channel estimation problem for the RIS-assisted wireless communication system under a time-variant scenario. A feasible transmission protocol is first proposed, and the cascaded channel is modeled as a state-space model. Kalman filter is employed in our model to estimate the time-varying channel by tracking the channel correlation and the channel's prior information. Based on the MMSE criterion, the optimal reflection coefficient matrix is derived to improve estimation accuracy. Numerical results prove that the proposed methods can bring significant gain if compared with the traditional estimators.

ACKNOWLEDGEMENT

This work was supported in part by National Natural Science Foundation of China (Grant Nos. 61921003, 61925101, 61831002 and 61901315), in part by the

Beijing Natural Science Foundation under (Grant No. JQ18016), and in part by the Fundamental Research Funds for the Central Universities (Grant No. 2020RC08).

References

[1] S. Gong, X. Lu, *et al.*, "Toward smart wireless communications via intelligent reflecting surfaces: A contemporary survey," *IEEE Communications Surveys & Tutorials*, vol. 22, no. 4, 2020, pp. 2283–2314.

[2] E. Basar, M. Di Renzo, *et al.*, "Wireless communications through reconfigurable intelligent surfaces," *IEEE Access*, vol. 7, 2019, pp. 116 753–116 773.

[3] Z. Zhao, Z. Ding, *et al.*, "Edge artificial intelligence in 6g systems: Theory, key techniques, and applications," *China Communications*, vol. 17, no. 8, 2020, pp. iii–iv.

[4] M. Di Renzo, A. Zappone, *et al.*, "Smart radio environments empowered by reconfigurable intelligent surfaces: How it works, state of research, and the road ahead," *IEEE Journal on Selected Areas in Communications*, vol. 38, no. 11, 2020, pp. 2450–2525.

[5] W. Tang, J. Y. Dai, *et al.*, "Mimo transmission through reconfigurable intelligent surface: System design, analysis, and implementation," *IEEE Journal on Selected Areas in Communications*, vol. 38, no. 11, 2020, pp. 2683–2699.

[6] C. Liaskos, S. Nie, *et al.*, "A new wireless communication paradigm through software-controlled metasurfaces," *IEEE Communications Magazine*, vol. 56, no. 9, 2018, pp. 162–169.

[7] Q. Wu and R. Zhang, "Towards smart and reconfigurable environment: Intelligent reflecting surface aided wireless network," *IEEE Communications Magazine*, vol. 58, no. 1, 2020, pp. 106–112.

[8] S. Li, B. Duo, *et al.*, "Reconfigurable intelligent surface assisted uav communication: Joint trajectory design and passive beamforming," *IEEE Wireless Communications Letters*, vol. 9, no. 5, 2020, pp. 716–720.

[9] Q. Tao, J. Wang, *et al.*, "Performance analysis of intelligent reflecting surface aided communication systems," *IEEE Communications Letters*, vol. 24, no. 11, 2020, pp. 2464–2468.

[10] Q. Wu and R. Zhang, "Intelligent reflecting surface enhanced wireless network via joint active and passive beamforming," *IEEE Transactions on Wireless Communications*, vol. 18, no. 11, 2019, pp. 5394–5409.

[11] C. Huang, A. Zappone, *et al.*, "Achievable rate maximization by passive intelligent mirrors," in *2018 IEEE International Conference on Acoustics, Speech and Signal Processing (ICASSP)*. IEEE, 2018, pp. 3714–3718.

[12] C. Huang, A. Zappone, *et al.*, "Reconfigurable intelligent surfaces for energy efficiency in wireless communication," *IEEE Transactions on Wireless Communications*, vol. 18, no. 8, 2019, pp. 4157–4170.

[13] S. Zhang and R. Zhang, "Capacity characterization for intelligent reflecting surface aided mimo communication," *IEEE Journal on Selected Areas in Communications*, vol. 38, no. 8, 2020, pp. 1823–1838.

[14] Zheng, P. Chu, *et al.*, "Intelligent reflecting surfaces enabled cognitive internet of things based on practical pathloss model," *China Communications*, vol. 17, no. 12, 2020, pp. 1–16.

[15] B. Zheng and R. Zhang, "Intelligent reflecting surface-enhanced ofdm: Channel estimation and reflection optimization," *IEEE Wireless Communications Letters*, vol. 9, no. 4, 2020, pp. 518–522.

[16] Y. Yang, B. Zheng, *et al.*, "Intelligent reflecting surface meets ofdm: Protocol design and rate maximization," *IEEE Transactions on Communications*, vol. 68, no. 7, 2020, pp. 4522–4535.

[17] Z.-Q. He and X. Yuan, "Cascaded channel estimation for large intelligent metasurface assisted massive mimo," *IEEE Wireless Communications Letters*, vol. 9, no. 2, 2020, pp. 210–214.

[18] H. Liu, X. Yuan, *et al.*, "Matrix-calibration-based cascaded channel estimation for reconfigurable intelligent surface assisted multiuser mimo," *IEEE Journal on Selected Areas in Communications*, vol. 38, no. 11, 2020, pp. 2621–2636.

[19] P. Wang, J. Fang, *et al.*, "Compressed channel estimation for intelligent reflecting surface-assisted millimeter wave systems," *IEEE Signal Processing Letters*, vol. 27, 2020, pp. 905–909.

[20] A. M. Elbir, A. Papazafeiropoulos, *et al.*, "Deep channel learning for large intelligent surfaces aided mm-wave massive mimo systems," *IEEE Wireless Communications Letters*, vol. 9, no. 9, 2020, pp. 1447–1451.

[21] G. Yu, X. Chen, *et al.*, "Design, analysis, and optimization of a large intelligent reflecting surface-aided b5g cellular internet of things," *IEEE Internet of Things Journal*, vol. 7, no. 9, 2020, pp. 8902–8916.

[22] C. Komninakis, C. Fragouli, *et al.*, "Multi-input multi-output fading channel tracking and equalization using kalman estimation," *IEEE Transactions on Signal Processing*, vol. 50, no. 5, 2002, pp. 1065–1076.

[23] T. Y. Al-Naffouri, "An em-based forward-backward kalman filter for the estimation of time-variant channels in ofdm," *IEEE Transactions on Signal Processing*, vol. 55, no. 7, 2007, pp. 3924–3930.

[24] Z. Wang, F. Yang, *et al.*, "Joint design of coalition formation and semi-blind channel estimation in fog radio access networks," *China Communications*, vol. 16, no. 11, 2019, pp. 1–15.

[25] S. M. Kay, *Fundumentals of Statistical Signal Processing: Estimation Theory*. NJ: Prentice-Hall, 1993.

Biographies

Zhendong Mao received his B.S degree in Applied Physics from Beijing University of Posts and Telecommunications, Beijing, China, in 2013. He is currently pursuing his Ph. D. degree at the State Key Laboratory of Networking and Switching Technology at BUPT. His current research interests including channel estimation, signal detection, deep learning and fog radio access networks.

Mugen Peng received the Ph.D. degree in communication and information systems from the Beijing University of Posts and Telecommunications (BUPT), Beijing, China, in 2005. Afterward, he joined BUPT, where he has been a Full Professor with the School of Information and Communication Engineering since 2012. He has been an Academic Visiting Fellow with Princeton University, Princeton, NJ, USA, since 2014. He has authored and coauthored over 100 refereed IEEE journal papers and over 300 conference proceeding papers. His main research areas include wireless communication theory, radio signal processing, cooperative communication, self-organization networking, heterogeneous networking, cloud communication, and Internet of Things. Prof. Peng was a recipient of the 2018 Heinrich Hertz Prize Paper Award; the 2014 IEEE ComSoc AP Outstanding Young Researcher Award; and the Best Paper Award in the JCN 2016 IEEE WCNC 2015, IEEE GameNets 2014, IEEE CIT 2014, ICCTA 2011, IC-BNMT 2010, and IET CCWMC 2009. He is on the Editorial/Associate Editorial Board of the IEEE Communications Magazine, IEEE Access, the IEEE Internet of Things Journal, IET Communications, and China Communications. He is the Fellow of IEEE and IET.

Xiqing Liu received the M.Sc. and Ph.D. degrees from the Harbin University of Science and Technology and Harbin Institute of Technology, Harbin, China, in 2012 and 2017, respectively. From 2018 to 2019, he was a Postdoctoral Fellow with the Department of Engineering Science, National Cheng Kung University, Taiwan, China. Currently, he is an Associate Research Fellow at the State Key Laboratory of Networking and Switching Technology (SKL-NST), School of Information and Communication Engineering, Beijing University of Posts and Telecommunications (BUPT), China. His current research interests include interference suppression in multicarrier systems, non-orthogonal multiple access and MIMO technologies.